Aerospace Science and Technology 155 (2024) 109611

Contents lists available at ScienceDirect

Aerospace Science and Technology

journal homepage: www.elsevier.com/locate/aescte

Aerodynamic shape optimization in transonic conditions through parametric model embedding

Andrea Serani [a,*], Matteo Diez [a], Domenico Quagliarella [b]

[a] CNR-INM, National Research Council–Institute of Marine Engineering, Rome, Italy
[b] CIRA, Italian Aerospace Research Centre, Capua, Italy

ARTICLE INFO

Communicated by Antonio Filippone

Keywords:
Parametric model embedding
Dimensionality reduction
Shape optimization
Aerodynamic design
Principal component analysis
Representation learning
Simulation-based design

ABSTRACT

The paper presents a novel approach for aerodynamic shape optimization problems using the parametric model embedding (PME) method. PME reduces the design-space dimensionality while maintaining a connection to the original design parameters, addressing the curse of dimensionality. The optimization of an airfoil's drag in transonic conditions demonstrates the method, using the RAE-2822 airfoil at Mach 0.734 and a Reynolds number of 6.5 million. Employing the covariance matrix adaptation evolution strategy, the process is performed with 1,000 function evaluations in both original and PME-reduced design spaces. Moreover, statistical criteria based on advanced risk function are introduced to characterize and study the evolution of the optimization process. Results show that PME effectively retains essential design space characteristics, capturing at least 95% of the geometric variance associated with the original design space. This leads to significant aerodynamic improvements, including reduced drag and smoother pressure distributions. Additionally, the statistical analysis helps to understand the advantages and disadvantages of different levels of parameter space compression.

1. Introduction

Despite significant advancements in computational capabilities over the past decade, shape design remains challenging, especially when relying on high-fidelity computational solvers. The pursuit of unique and innovative designs often leads to exploring larger design spaces, but this exacerbates the curse of dimensionality (CoD) [3], a well-known problem in global optimization where the performance of optimization algorithms and surrogate models deteriorate as the design space dimension increases. In industrial design, where time is a limited resource, techniques that reduce the computational demands of simulation-based design optimization (SBDO) [35] are essential for improving efficiency and meeting tight deadlines. Among the others, design-space dimensionality reduction approaches [33] are those methods capable of alleviating the CoD, while preserving an accurate representation of the original design parameterization.

The easiest method for reducing the design-space dimensionality is through the so-called indirect methods, such as factor screening [22], which involves identifying the most significant variables for the design problem and fixing the remaining ones to constant values during optimization. However, this approach can be limiting as it does not consider the impact that fixed variables could have when combined with other variables. A more comprehensive evaluation can be done through variance-based sensitivity analysis using, e.g., Sobol indices [36]. However, this method operates within a probabilistic framework and requires a large number of design space samples, which can be computationally expensive. Additionally, the number of indices increases with the design space dimensionality. For this reason, direct approaches, that address the dimensionality reduction process through re-parameterization, have increased their popularity, especially in the aeronautic domain [33]. Leveraging on machine learning principle [18], direct design-space dimensionality reduction approaches are classified as representation learning methods [4], that can identify important structures in the design-space parameterization.

One such method, based on the proper orthogonal decomposition (POD), equivalent to Karhunen-Loève expansion (KLE) [8], was developed to assess shape modification variability and create a reduced-dimensionality model of the shape modification vector. This method does not require objective function evaluations or gradients. It operates by applying POD/KLE to the shape modification vector only, and after discretizing the equations, it reduces to the principal component analysis (PCA) of discrete geometrical data. The method enhances shape

* Corresponding author.
E-mail address: andrea.serani@cnr.it (A. Serani).
URL: https://www.inm.cnr.it (A. Serani).

https://doi.org/10.1016/j.ast.2024.109611
Received 31 July 2024; Received in revised form 18 September 2024; Accepted 19 September 2024
Available online 24 September 2024

Nomenclature

$\mathbf{d}$	shape modification vector	$\mathbf{P}$	PME data matrix
$\mathbf{g}, \mathbf{g}'$	original, deformed shape/geometry	$\widetilde{\mathbf{W}}$	PME weights matrix
$\mathbf{u}$	design variables vector/original parameterization	c	airfoil chord length
$\check{\mathbf{u}}$	reconstructed design variables vector	r	leading edge radius
$\mathbf{x}$	reduced design variables vector/reduced paramaterization	t, t_{85}	airfoil thickness, thickness at 85% of c
$\mathbf{y}$	operational conditions	C_D	drag coefficient
$\mathbf{v}_k$	PME eigenvector component associated to $\mathbf{u}$	C_L	lift coefficient
$\mathbf{z}_k$	PME eigenvector component associated to $\mathbf{d}$	C_M	pitching moment coefficient
$\widetilde{\mathbf{z}}_k$	PME eigenvector	C_p	pressure coefficient
$\mathcal{G}$	manifold identifying the original shape/geometry	CVaR	conditional value-at-risk
α	angle of attack	L	shape discretization size
$\boldsymbol{\delta}$	shape modification function	M	number of original design variables
λ_k	PME eigenvalues	N	number of reduced design variables
σ^2	geometric variance	S	number of Monte Carlo items
τ	trailing edge angle	$\langle\cdot\rangle$	ensemble average
$\boldsymbol{\xi}$	curvilinear coordinates on $\mathcal{G}$		

optimization efficiency through re-parameterization and dimensionality reduction, providing a better understanding of the design space and shape parametrization before optimization or performance analysis. This method, also known as modal parameterization [18], has been crucial in enhancing the design of airfoils and wings, streamlining external aerodynamic optimizations in subsonic [6,17,46], transonic [2,19,21,24–26,38–40,42,45], and hypersonic [20] regimes of airfoils and wings, as well as for internal aerodynamics of compressors [44,47], turbines [13], and nozzles [43].

However, the standard POD/PCA-based dimensionality reduction approaches have a significant limitation: they cannot explicitly reconstruct the original parameterization. This limitation, known as the pre-image problem [9], arises because when shape data is reduced into a set of principal components, the resulting low-dimensional representation lacks a direct mapping to the original shape parameters that designers use. In industrial design, the original shape parameters (e.g., airfoil coordinates or wing section definitions) have a clear geometric meaning, which is preferred for ease of interpretation and adjustment. Unfortunately, traditional POD/PCA methods do not preserve this original parameterization in the reduced space, making it difficult to reverse the dimensionality reduction process and recover the exact original shape from the principal components. This disconnect complicates the use of these methods in industrial applications, where designers need the ability to interpret and modify designs in terms of their original parameters.

The parametric model embedding (PME) [32] technique was recently developed by the authors and aims to enhance the efficiency of shape optimization processes. PME can reduce the size of the design space while maintaining an explicit connection to the original parameters, such as the geometric and design variables that define the shape. Specifically, these parameters could include control points of a spline, airfoil coordinates, or any other parameters that directly describe the geometry or configuration of the design in question. The explicit connection refers to the fact that PME does not lose or obscure these original geometric descriptors during the dimensionality reduction process, unlike standard POD/PCA approaches. The PME method creates a reduced design space that still retains a direct link to these original shape and design variables, which allows for both an efficient optimization process and an intuitive understanding of how the shape modifications affect the design in the original parametric space. It achieves this by incorporating a more comprehensive feature space that includes both the shape modification vectors and the design variables themselves. PME uses a generalized inner product to properly resolve the prescribed design variability, selecting a latent dimensionality that best captures the essence of the shape changes while preserving the interpretability of the original parameters. This enables designers to manipulate the design in a reduced space while still understanding its impact on the physical geometry or configuration.

The primary objective of this work is to introduce and validate a novel approach to aerodynamic shape optimization by leveraging PME for design-space re-parameterization. This involves the application of statistical criteria based on advanced risk functions to characterize and study the evolution of the optimization process, highlighting that a very effective parameter compression does not necessarily lead to a more efficient optimization procedure.

To achieve a meaningful statistical analysis, significant computational resources were invested. The analysis was performed on a statistical sample, requiring multiple runs of the optimization process with different initial conditions of the evolutionary algorithm. Each optimization process utilized Reynolds-averaged Navier-Stokes (RANS) solvers on a converged mesh, demanding substantial computational power.

Another novelty of this paper is that the computational chain used is entirely based on open-source components (see gitlab.com/qudo046/avt-331-l-2-aero-benchmarks.git). This allows other researchers to examine the results or verify their algorithms on problems similar to those of industrial interest.

The remainder of the article is organized as follows: section 2 presents the PME formulation; section 3 is devoted to introducing the aerodynamic shape optimization problem, with details on the shape parametrization methods, the numerical solver, and the computational grid, as well as a description of the optimization algorithm; the results are presented and discussed in section 4 and 5; finally, section 6 provides conclusions and future perspectives.

2. Parametric model embedding

Design-space dimensionality reduction using POD or PCA has demonstrated its effectiveness in reducing dimensionality prior to the optimization loop, thereby mitigating the CoD associated with the optimization problem [33]. However, when the dimensionality reduction procedure relies solely on the shape modification vector, it does not inherently offer a method to revert to the original design variables from the latent space, which is the reduced dimensional representation of the original shape parameterization. This leads to two significant challenges:

1. the POD/PCA modal parameterization necessitates the implementation of a new shape modification method based on the POD/PCA eigenvectors;
2. when fewer than all POD/PCA modes are used (as is typical in dimensionality reduction), there is no guarantee that the shape

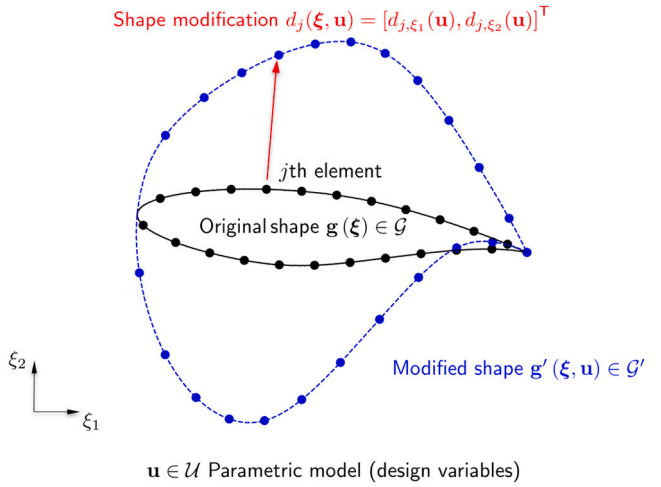

Fig. 1. Shape modification example and notation for $n = 2$.

produced using these reduced eigenvectors will reside within the original design space, potentially resulting in infeasible designs.

The PME technique has been developed to address these limitations [32]. PME extends standard PCA-based dimensionality reduction by incorporating the design variables into a generalized feature space formed by both the discretized shape deformation vector $\mathbf{d}$ and the original design variables $\mathbf{u}$. This approach ensures a more robust and feasible mapping between the reduced design space and the original design space, facilitating effective and practical shape optimization.

Consider a manifold $\mathcal{G}$, which identifies the original/parent shape, whose coordinates in the nD-space are represented by $\mathbf{g}(\boldsymbol{\xi}) \in \mathbb{R}^n$ with $n = 1, 2$, or 3; $\boldsymbol{\xi} \in \mathcal{G}$ are curvilinear coordinates defined on $\mathcal{G}$. Assume that, for the purpose of shape optimization, $\mathbf{g}$ can be transformed to a deformed shape/geometry $\mathbf{g}'(\boldsymbol{\xi},\mathbf{u})$ by

$$\mathbf{g}'(\boldsymbol{\xi},\mathbf{u}) = \mathbf{g}(\boldsymbol{\xi}) + \boldsymbol{\delta}(\boldsymbol{\xi},\mathbf{u}) \qquad \forall \boldsymbol{\xi} \in \mathcal{G} \tag{1}$$

where $\boldsymbol{\delta}(\boldsymbol{\xi},\mathbf{u}) \in \mathbb{R}^n$ is the resulting shape modification vector, defined by arbitrary shape parameterization or modification method (e.g., CAD parameterization, Bezier surfaces, FFD, NURBS, etc.), and $\mathbf{u} \in \mathcal{U} \subset \mathbb{R}^M$ is the design variable vector. Fig. 1 shows an example of the current notation for $n = 2$.

Discretizing $\mathcal{G}$ by L elements of measure $\Delta\mathcal{G}_j$ (with $j = 1, \dots, L$), having $\mathbf{d}(\boldsymbol{\xi},\mathbf{u})$ as the discretization of $\boldsymbol{\delta}(\boldsymbol{\xi},\mathbf{u})$, sampling $\mathcal{U}$ by a statistically convergent number of Monte Carlo (MC) realizations S, so that $\{\mathbf{u}_k\}_{k=1}^S \sim p(\mathbf{u})$, and organizing the discretization $\hat{\mathbf{d}} = \mathbf{d} - \langle\mathbf{d}\rangle$ (with $\langle\cdot\rangle$ the ensemble average) in a data matrix $\mathbf{D}$ of dimensionality $[nL \times S]$

$$\mathbf{D} = \begin{bmatrix} \hat{d}_{1,\xi_1}(\mathbf{u}_1) & & \hat{d}_{1,\xi_1}(\mathbf{u}_S) \\ \vdots & & \vdots \\ \hat{d}_{L,\xi_1}(\mathbf{u}_1) & & \hat{d}_{L,\xi_1}(\mathbf{u}_S) \\ \vdots & \cdots & \vdots \\ \hat{d}_{1,\xi_n}(\mathbf{u}_1) & & \hat{d}_{1,\xi_n}(\mathbf{u}_S) \\ \vdots & & \vdots \\ \hat{d}_{L,\xi_n}(\mathbf{u}_1) & & \hat{d}_{L,\xi_n}(\mathbf{u}_S) \end{bmatrix} \tag{2}$$

where $\hat{d}_{j,\xi_k}$ is the k-th component of the shape modification vector associated to the j-th element, defining $\hat{\mathbf{u}} = \mathbf{u} - \langle\mathbf{u}\rangle$, the embedding is achieved introducing a matrix $\mathbf{P}$ of dimensionality $[(nL + M) \times S]$ as follows

$$\mathbf{P} = \begin{bmatrix} \mathbf{D} \\ \mathbf{U} \end{bmatrix} \qquad \text{with} \qquad \mathbf{U} = \begin{bmatrix} \hat{u}_{1,1} & & \hat{u}_{1,S} \\ \vdots & \cdots & \vdots \\ \hat{u}_{M,1} & & \hat{u}_{M,S} \end{bmatrix} \tag{3}$$

where the matrix $\mathbf{U}$ is added to the data matrix $\mathbf{D}$ with a null weight $\mathbf{W}_\mathbf{u}$ such that

$$\mathbf{W}_\mathbf{u} = \mathbf{0} \qquad \text{and} \qquad \widetilde{\mathbf{W}} = \begin{bmatrix} \mathbf{W} & \mathbf{0} \\ \mathbf{0} & \mathbf{W}_\mathbf{u} \end{bmatrix} \tag{4}$$

and so leading to a generalized PCA problem in the form

$$\widetilde{\mathbf{A}}\widetilde{\mathbf{G}}\widetilde{\mathbf{W}}\widetilde{\mathbf{Z}} = \widetilde{\mathbf{Z}}\widetilde{\boldsymbol{\Lambda}} \qquad \text{with} \qquad \widetilde{\mathbf{A}} = \frac{1}{S}\mathbf{P}\mathbf{P}^\mathsf{T} \tag{5}$$

where $\widetilde{\mathbf{Z}}$ and $\widetilde{\boldsymbol{\Lambda}}$ represent the eigenvectors and eigenvalues matrices of $\widetilde{\mathbf{A}}\widetilde{\mathbf{G}}\widetilde{\mathbf{W}}$, where

$$\widetilde{\mathbf{G}} = \begin{bmatrix} \mathbf{G} & \mathbf{0} \\ \mathbf{0} & \mathbf{I} \end{bmatrix} \tag{6}$$

and

$$\widetilde{\mathbf{Z}} = \begin{bmatrix} \tilde{\mathbf{z}}_1 & \dots & \tilde{\mathbf{z}}_S \end{bmatrix} \qquad \text{with} \qquad \tilde{\mathbf{z}}_k = \begin{bmatrix} \mathbf{z}_k \\ \mathbf{v}_k \end{bmatrix} \tag{7}$$

The matrix $\mathbf{G} = \text{diag}\left(\mathbf{G}_1, \dots, \mathbf{G}_n\right)$ is block diagonal and has dimensionality $[nL \times nL]$, with each $[L \times L]$ k-th block being a diagonal matrix itself

$$\mathbf{G}_k = \text{diag}\left(\Delta\mathcal{G}_1, \dots, \Delta\mathcal{G}_L\right) \tag{8}$$

containing the measure $\Delta\mathcal{G}_j$ of the j-th element. Similarly, $\mathbf{W} = \text{diag}\left(\mathbf{W}_1, \dots, \mathbf{W}_n\right)$ is a block diagonal matrix of dimensionality $[nL \times nL]$, where each $[L \times L]$ k-th block $\mathbf{W}_k$ $(k = 1, \dots, n)$ is itself a diagonal matrix defined as

$$\mathbf{W}_k = \text{diag}\left(\rho_1, \dots, \rho_L\right) \tag{9}$$

with ρ_j (for $j = 1, \dots, L$) the arbitrary weight given to each element.

Having given a null weight to $\mathbf{U}$ does not remove the contribution of the design variables from the inner product, but just cancels as many columns as M from the matrix $\widetilde{\mathbf{A}}\widetilde{\mathbf{G}}\widetilde{\mathbf{W}}$.

The solutions λ_k and $\mathbf{z}_k$ of Eq. (5) are finally used to construct the reduced dimensionality representation of the original parameterization; defining the desired confidence level l, with $0 < l \leq 1$, the number of reduced design variables N is chosen such that

$$\sum_{k=1}^{N} \lambda_k \geq l \sum_{k=1}^{nL} \lambda_k = l\sigma^2 \quad \text{with} \quad \lambda_k \geq \lambda_{k+1} \tag{10}$$

and the PME of the original design variables is finally achieved by

$$\mathbf{u} \approx \breve{\mathbf{u}} = \langle\mathbf{u}\rangle + \sum_{k=1}^{N} x_k \mathbf{v}_k \tag{11}$$

where the eigenvectors component $\mathbf{v}_k$ embeds (or contains) the reduced-order representation of the original design parameterization.

To reconstruct at least all the samples in $\mathbf{D}$, the coefficients θ_j, for $j = 1, \dots, S$, are evaluated projecting the matrix $\mathbf{P}$ on $\widetilde{\mathbf{Z}}'$, that contains only the first N eigenvectors of $\widetilde{\mathbf{Z}}$, retaining the desired level of variance of the original design space, as follows

$$\boldsymbol{\Theta} = \mathbf{P}^\mathsf{T}\widetilde{\mathbf{G}}\widetilde{\mathbf{W}}\widetilde{\mathbf{Z}}' \tag{12}$$

with $\boldsymbol{\Theta} = [\theta_1 \ \dots \ \theta_S]^\mathsf{T}$. Consequently, the reduced design variables $\mathbf{x} = [x_1 \ \dots \ x_N]^\mathsf{T}$ can be bounded such as

$$\min_j \Theta_{jk} \leq x_k \leq \max_j \Theta_{jk} \qquad k = 1, \dots N. \tag{13}$$

It may be noted that the overall methodology is independent of the specific shape modification method, which is seen as a black box by PME. Fig. 2 shows the extended design matrix structure (XDSM) [16] of the SBDO process integrating the PME method. It may be noted that the PME is performed offline/upfront to the optimization procedure and this is given by assigning a negative sign to the associated XDSM blocks.

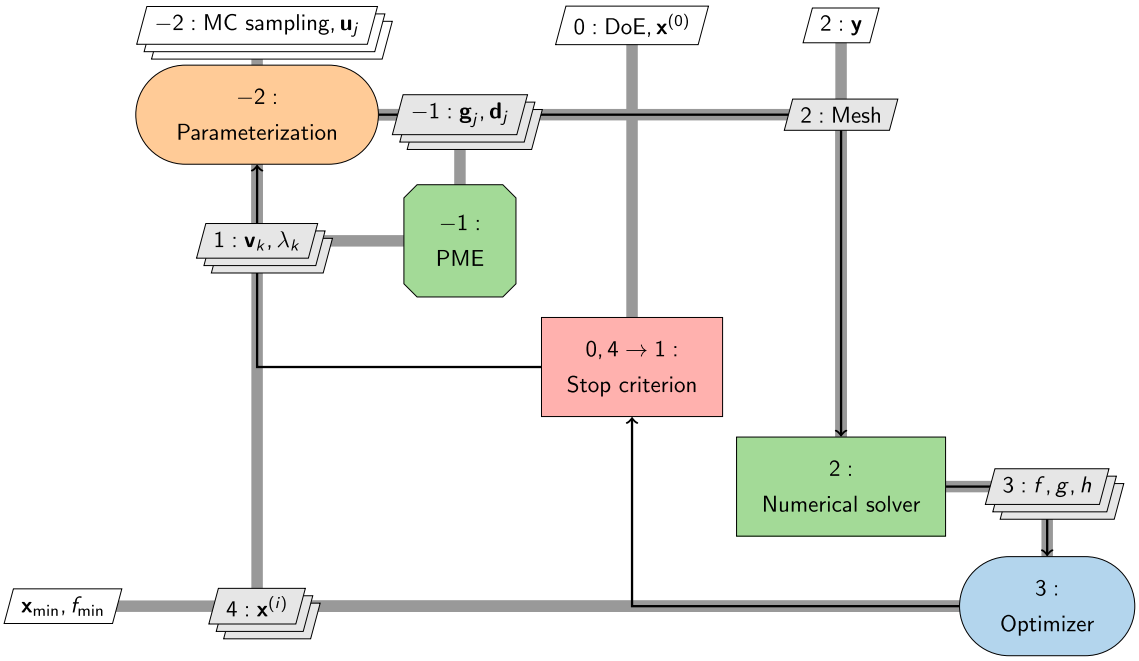

Fig. 2. XDSM diagram for the solution of a shape optimization by PME.

3. Aerodynamic shape optimization problem

The study focuses on the shape re-parameterization and optimization of the RAE-2822 airfoil in transonic conditions using PME. The airfoil operates under conditions of Mach 0.734 and a Reynolds number of 6.5×10^6. The design optimization problem is defined as follows:

$$\begin{array}{rl} \text{minimize} & C_D(\mathbf{u}) \\ \text{subject to} & C_L(\mathbf{u}) = 0.824 \\ \text{and to} & -0.11 \le C_M \le -0.01 \\ & t/c = 0.1211 \\ & r \ge 0.007c \\ & \tau \ge 5° \\ & t_{85}/c \ge 0.02 \\ & \mathbf{u}_l \le \mathbf{u} \le \mathbf{u}_u, \end{array} \tag{14}$$

where C_D is the drag coefficient and c is the airfoil chord. The lift coefficient (C_L) constraint is maintained by treating the angle of attack (α) as a free parameter, which is automatically managed by the flow analysis driver. In this design optimization problem, constraints are imposed for the pitching moment (C_M), the maximum thickness-to-chord ratio (t/c), the leading-edge radius (r), the trailing edge angle (τ), and the thickness at 85% of the chord (t_{85}/c).

The shape handler ensures that the maximum thickness constraint is automatically satisfied by scaling the airfoil following its parametric modification. These constraints ensure the aerodynamic performance and structural integrity of the optimized airfoil [34]. The proposed problem is similar to the AIAA Aerodynamic Design Optimization Discussion Group (ADODG)[1] case 2; however, some differences make the problem slightly more difficult. In particular, a constraint on the maximum thickness, which is fixed and must be equal to that of RAE-2822, substitutes the constraint on the minimum area of the airfoil, and other geometric constraints are imposed on the minimum thickness at 85% of the chord and leading-edge radius.

[1] https://sites.google.com/view/mcgill-computational-aerogroup/adodg.

3.1. Shape parameterization

The design space was defined within the activities of the NATO-AVT-331 [5] and is composed of $M = 20$ design variables, each linked to a different shape function (see Fig. 3) that operates either on the upper or lower side of the airfoil [28]. Namely, the shape modification functions include 6 polynomials, 12 Hicks-Henne bumps, and 2 Wagner functions [12].

An in-house code (WG2AER developed at CIRA) parameterizes the airfoil as a linear combination of the parent geometry $\mathbf{g}(\boldsymbol{\xi})$, and the modification functions $\boldsymbol{\delta}$.

3.2. Numerical solver and computational grid

The flow solver used to obtain RANS solutions is the open-source finite-volume code SU2 [23] v6.2.0, conceived at Stanford University and steadily growing in diffusion in the aeronautical world thanks to a broad community of developers active all over the world. SU2 is written in C++ language and is characterized by a highly modular structure that is easily extensible for the solution of any set of PDE. The heart of the software is the parallel RANS solver capable of solving problems of interest to the mechanical and aerospace industry in the turbulent transonic regime.

The present work uses the Spalart-Allmaras turbulence model [37] along with a 2nd-order monotone upstream-centered scheme for conservation law and an adaptive Courant–Friedrichs–Lewy number.

The numerical solution of the RANS equations using the finite volume method requires the generation of computational meshes with carefully specified characteristics. Indeed, in the context of optimization, it is not enough to generate a calculation grid for a single geometry. Furthermore, it is necessary to have an automatic procedure able to generate a calculation grid for each new geometry that the optimizer needs to analyze. The implementation of this type of procedure is not trivial because it is necessary to find a compromise between calculation accuracy, fast CFD computation, and the robustness of the meshing procedure to minimize errors that could occur during the grid generation phase. The automated procedure here presented takes in input the airfoil points, some flow data, and some grid control parameters, and returns a hybrid grid composed of triangles and quadrangles in the format suitable for SU2 solver.

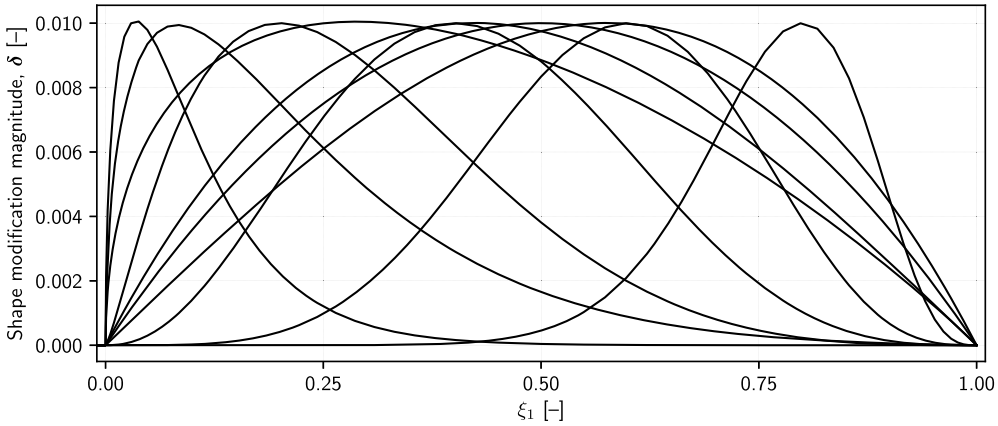

Fig. 3. Shape modification functions of the parametric model.

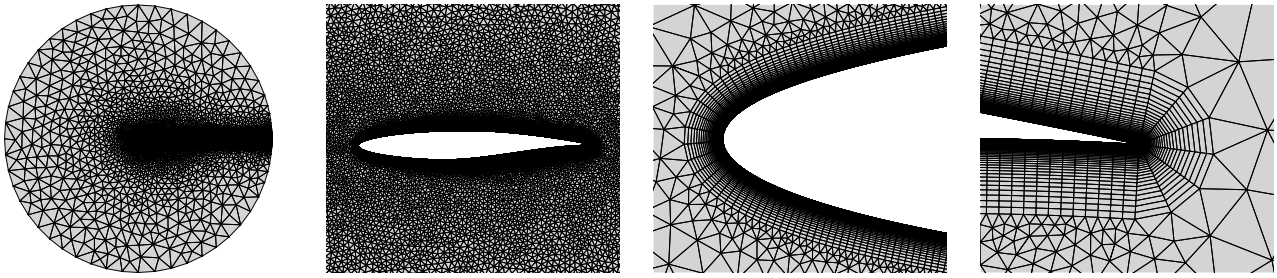

Fig. 4. RAE 2822 computational domain and grid details.

The grid generation engine is the GMSH v4 software [10] that is excellent in terms of efficiency and robustness and batch usage capabilities. The interface script to GMSH requires as input, basically, the coordinates of the airfoil, the dimensions of the fluid domain, the Reynolds number, and a reference length. According to input data, a hybrid grid with proper and accurate modeling of the boundary layer and the wake is obtained. The parametric mesh generation procedure uses the field feature of GMSH to manage cell sizes and refinement zones, like the wake and the boundary layer.

It is worth noting that, for unstructured grids, mesh deformation techniques are often preferred in literature over computational mesh regeneration. Here, instead, mesh regeneration is considered to be a more practical solution. Indeed, both methods offer advantages and disadvantages: for example, mesh deformation more reliable when it comes to computing the finite difference gradient of the quantity of interest, while re-meshing allows better control of the quality of the grid when it is necessary to explore a fairly large set of variations in the space of the design parameters, as is typical of many evolutionary algorithms and when one wants, as in our case, to explore the impact on the parameterization on a large set of possible shapes.

A circular computational domain with a radius equivalent to $40c$ is used. The computational grid is hybrid, with a mix of quadrilateral (quad) and triangular (tri) elements. The quad elements are used in the boundary layer region whose height is estimated using the Schlichting formula for turbulent boundary layer on a flat plate. This leads to about 57k mesh elements to discretize the boundary layer region. The first cell height (adjacent to the airfoil surface) is calculated to approximatively respect the condition that the dimensionless distance from the wall $y^+ = yu_\tau/\nu$ is ≈ 1, with u_τ friction velocity and ν kinematic viscosity. The remaining part of the flow field is discretized using tri elements, and about 97k cells are used for a total of about 160k mesh elements. An example of an automatically generated grid for the RAE-2822 airfoil is shown in Fig. 4, where the detail of the boundary layer zone and the treatment of the corner point at the trailing edge are shown.

3.3. Optimization algorithm

The covariance matrix adaptation evolution strategy (CMA-ES) is a robust stochastic optimization algorithm, particularly effective for non-linear or non-convex optimization problems. It belongs to the family of evolutionary algorithms, employing a population-based approach to optimize a given objective function. The algorithm maintains and adapts a distribution of candidate solutions using a multivariate normal distribution [11].

The update rules of the CMA-ES rely on the mean vector $\mathbf{m}_t$ and the covariance matrix $\mathbf{C}_t$ of the distribution. The algorithm initializes the mean $\mathbf{m}_0$, covariance matrix $\mathbf{C}_0 = \mathbf{I}$, step size σ_0, and other internal parameters like evolution paths. Generating a new population of γ candidate solutions from the current normal distribution:

$$\mathbf{x}_k = \mathbf{m}_t + \sigma_t \mathbf{C}_t^{1/2} \mathbf{r}_k \quad \text{for } k = 1, \dots, \gamma, \tag{15}$$

where $\mathbf{r}_k \sim \mathcal{N}(\mathbf{0}, \mathbf{I})$ is a standard normal random vector, CMA-ES evaluates each candidate solution using the objective function. Selecting the top μ candidates based on their objective values to form the new mean:

$$\mathbf{m}_{t+1} = \sum_{i=1}^{\mu} w_i \mathbf{x}_{i:\gamma}, \tag{16}$$

where $\mathbf{x}_{i:\gamma}$ is the i-th best candidate and w_i is the corresponding weight, the algorithm updates the evolution paths $\mathbf{p}_c$ and $\mathbf{p}_\sigma$ for step size and covariance matrix adaptation, respectively, and then updates the covariance matrix $\mathbf{C}_t$:

$$\mathbf{C}_{t+1} = (1 - c_1 - c_\mu)\mathbf{C}_t + c_1 \mathbf{p}_c \mathbf{p}_c^\top + c_\mu \sum_{i=1}^{\mu} w_i \mathbf{r}_{i:\gamma} \mathbf{r}_{i:\gamma}^\top. \tag{17}$$

Finally, the step size σ_t is updated using the evolution path $\mathbf{p}_\sigma$.

The adaptation of the covariance matrix enables CMA-ES to learn the underlying shape of the objective function and to conduct effec-

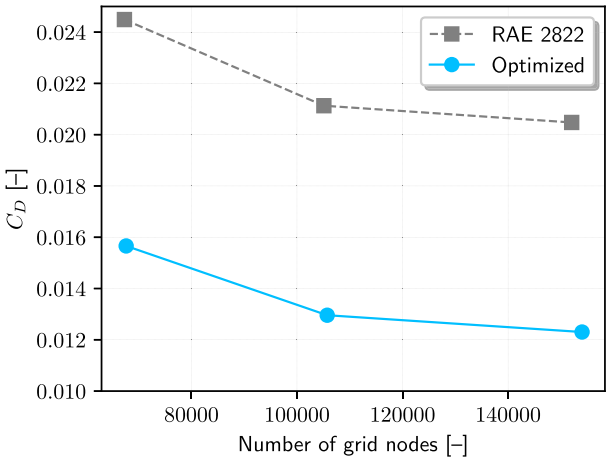

Fig. 5. Grid verification study for the original RAE 2822 and the optimized airfoils.

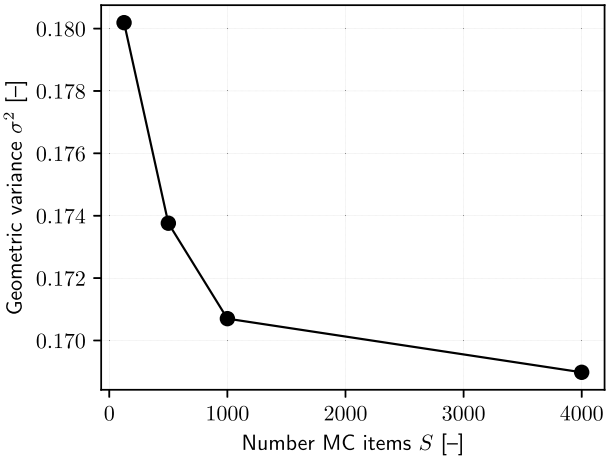

Fig. 6. Geometric variance convergence as a function of the MC items.

tive search strategies by adjusting the distribution of candidate solutions over successive generations.

4. Results

A preliminary evaluation of the computational grid for the parent airfoil was carried out through a grid verification study, following the methodology described in [41]. A grid triplet (G1, G2, G3) was established, where G1 comprises approximately 160k elements, while G2 and G3 are progressively coarser with refinement ratios of $r \approx 1.2$. Fig. 5 shows a monotonic convergence, as indicated by $R \approx 0.2$, which reflects the ratio of solution differences between the grid levels. This ratio being less than 1 confirms that the grid exhibits monotonic convergence. To account for the discretization error, the grid uncertainty was estimated using the grid convergence index method, yielding an uncertainty estimate of approximately 1.32%.

4.1. Design-space dimensionality reduction results

In previous studies [32], it has been demonstrated that a limited number of samples (on the order of a few thousand) is sufficient for PME training purposes. In this study, the geometric variance changes with a variation of less than 1% from 1,000 to 4,000 MC items (see Fig. 6). Therefore, the PME is trained by a set of $S = 4,000$ MC items as they provide convergence and are more than sufficient to ensure accuracy.

The geometry is discretized by $L = 364$ grid nodes, providing a data matrix $\mathbf{P}$ of dimension $[748 \times 4000]$. Fig. 7 shows the variance resolved

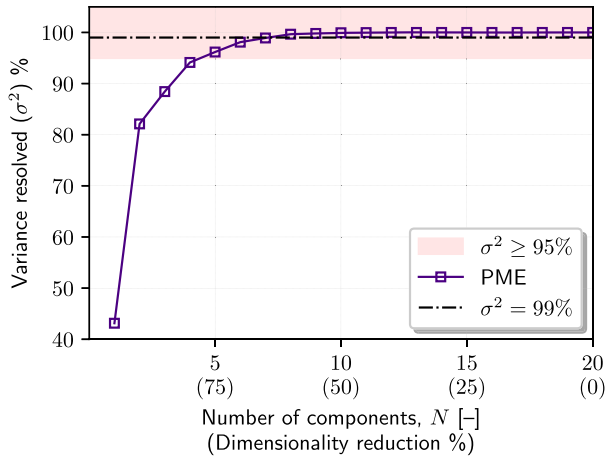

Fig. 7. Variance resolved as a function of the number of reduced design variables.

by PME. The number of reduced design variables to retain at least the 95% of the original geometric variance is equal to $N = 5$, achieving a dimensionality reduction equal to 75%, whereas $N = 8$ reduced-design variables, corresponding to a dimensionality reduction equal to 60%, are needed to retain at least the 99% of the original geometric variance. The corresponding eigenvectors $\mathbf{z}_k$ and $\mathbf{v}_k$ (for $k = 1, \dots, 8$) are shown in Fig. 8. Note that the PME eigenvector components for the shape representation $\mathbf{z}_k$ (see Fig. 8 left) are those obtained by lower and upper bound of $\boldsymbol{\Theta}$ (see Eq. (13)). These are not used for the shape modification in reduced design space, which is based on $\mathbf{v}_k$ (see Fig. 8 right) through the reconstruction of the original design variables via Eq. (11), but allows to understand what are the maximum allowable deformations with the reduced-design variables. Furthermore, $\mathbf{v}_k$ allows to understand what of the original design variables participate in the reduced design variables, e.g., looking at the peaks of $\mathbf{v}_1$, it is mostly participated by u_2, u_4, u_6, and u_{20}, and partially by u_{12}, u_{14}, and u_{16}.

Fig. 9 illustrates an example of geometry reconstruction. Specifically, it presents one variant among the 4,000 MC items in $\mathbf{D}$, originally parameterized by its shape and subsequently reconstructed via PME. The figure depicts the progression of PME reconstruction quality from left to right, showing improvements as the dimensionality N increases. It is evident that while $N = 5$ captures at least 95% of the original design variability, it still exhibits noticeable differences compared to the original geometry. In contrast, increasing N to 8, which covers 99% of the geometric variance, results in a significantly improved and accurate reconstruction.

4.2. Optimization results

The optimization problem defined in Eq. (14) is addressed using the CMA-ES. This is applied with a population size of 10 individuals, and the total computational budget is set to 1,000 function evaluations. The optimization process is carried out both in the original design space, which has a dimensionality of $M = 20$, and in two PME-reduced design spaces with dimensionalities of $N = 5$ and $N = 8$, respectively. Given the stochastic nature of CMA-ES, each optimization scenario is independently repeated 10 times to ensure statistical robustness.

Fig. 10 shows the optimization convergence, considering the best results over the 10 repetitions. The optimization performed in the reduced design space using $N = 5$ does not allow for achieving a better optimum compared to the optimization procedure conducted in the original design space. On the contrary, using $N = 8$ a better optimum is found. This last design space allows also for a slightly faster convergence towards the optimum, compared to the original design space. Detailed statistics on the optimization results a given in Table 1. The optimal (original) design variables are compared in Fig. 11, while the associated airfoil

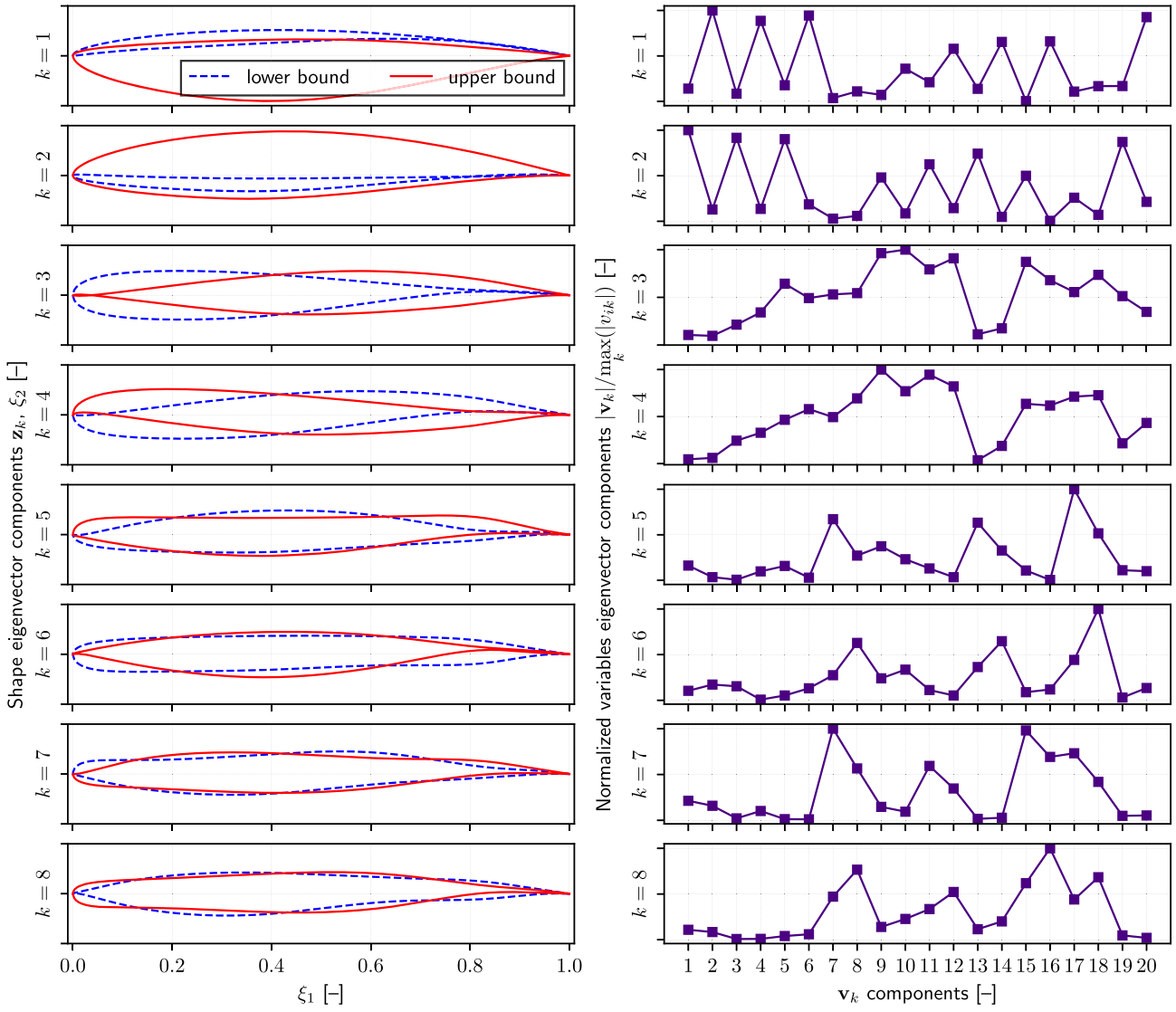

Fig. 8. Shape modification vector modes $\mathbf{z}_k$ on the left and embeddings modes $\mathbf{v}_k$ on the right, for $k = 1, \ldots, 8$ (from top to bottom).

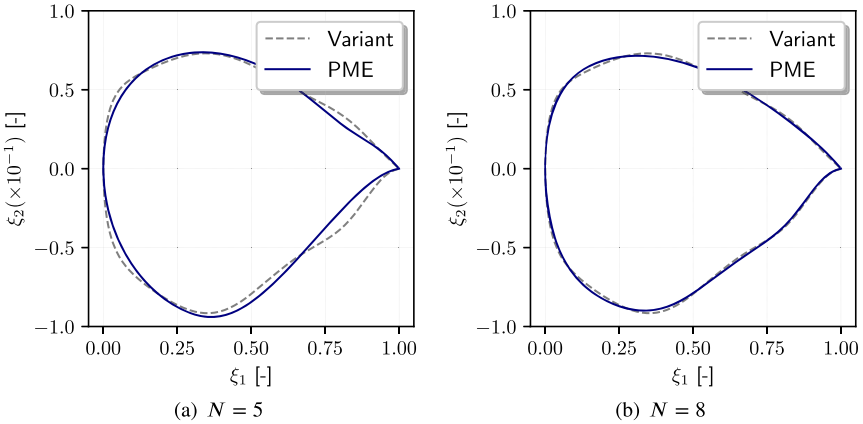

(a) $N = 5$ (b) $N = 8$

Fig. 9. Example of PME reconstruction of one airfoil variant, conditional to the number of reduced design variables N.

Table 1
Summary and statistics of the optimization results in terms of drag coefficient C_D.

Design space	Number of design variables	Worst	Median	Best	Best ΔC_D%
Original	$M = 20$	0.0126963	0.0125283	0.0124299	-39.3
PME (95%σ^2)	$N = 5$	0.0138232	0.0131226	0.0128821	-37.1
PME (99%σ^2)	$N = 8$	0.0129479	0.0126019	0.0123595	-39.7

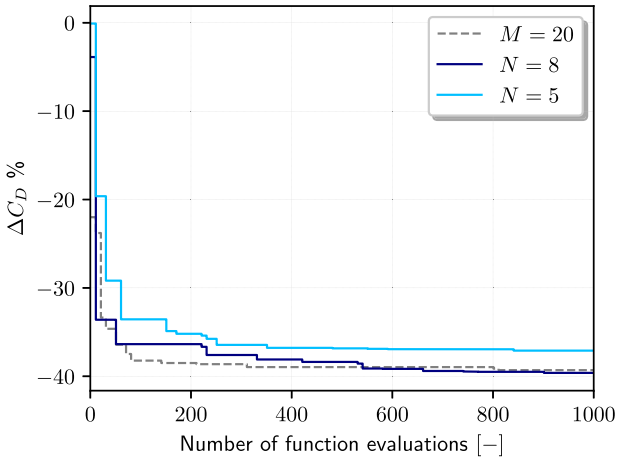

Fig. 10. Optimization convergence.

shapes and pressure coefficient C_p along the cord are shown in Fig. 12. The optimal design variables (see Fig. 11) are quite different, but not so far from the parent airfoil. Indeed, the differences in the optimal shapes (see Fig. 12 top) are not highly appreciable, especially when comparing $M = 20$ to $N = 5$. Major differences are visible for $N = 8$, compared to $M = 20$. Finally, looking both at the C_p and the Mach field (shown in Fig. 13) it can be seen that all the optimal designs have reduced the shock present on the parent airfoil and this is definitely smoother for $N = 8$, compared to the others.

Finally, a grid convergence study for the optimal configuration ($N = 8$ PME best) has been conducted, confirming that the mesh regeneration approach yields consistent and robust results. As shown in Fig. 5, the drag coefficient for the optimized airfoil converges similarly to the original RAE-2822 case, ensuring reliability in the optimization outcomes.

5. Discussion

To statistically assess the performance of the evolutionary algorithm's worst, median, and best values have been provided in Table 1, and optimization convergence, as well as optimal shapes, have been shown for the best results obtained using the three design spaces. Nevertheless, although the optimization runs were replicated 10 times each with different seeds, the benefits of using the reduced design spaces are not so clear, and a further discussion here is presented to understand how the different parameterization allowed more or less efficient exploration of the search space during the optimization process.

For this purpose, the single generation of individuals from each optimization run is extracted (including the initialization phase, in which fitness information is not yet used to direct the search) and grouped the homologous generations for each parameterization used. As can be observed from Fig. 14, the empirical distributions of the quantity of interest (QoI) to be optimized allow to evaluate how (on average) the individuals belonging to the i-th generation are distributed in the search space. Of particular interest are the tails of the distributions, which allow to compare how the elements of a given generation tend to distribute themselves around the minimum values (left tail) or how they tend to disperse in regions far from the optimum (right tail). To numerically evaluate these aspects of the empirical distribution, the conditional value-at-risk (CVaR, also defined in the literature as expected shortfall or superquantile, [1,29]) is used. Its definition for the left and right distribution tails, respectively left CVaR ($\mathrm{CVaR}^L_\alpha(X)$ or left-tail conditional expectation below $\mathrm{VaR}_\alpha(X)$) and right CVaR ($\mathrm{CVaR}^R_\alpha(X)$ or right-tail conditional expectation above $\mathrm{VaR}_\alpha(X)$), are defined as follows:

$$\mathrm{CVaR}^L_\alpha(X) = \mathrm{E}[X \mid X \le \mathrm{VaR}_\alpha(X)] = \frac{1}{\alpha}\int_0^\alpha \mathrm{VaR}_\gamma(X)\,d\gamma \tag{18}$$

$$\mathrm{CVaR}^R_\alpha(X) = \mathrm{E}[X \mid X \ge \mathrm{VaR}_\alpha(X)] = \frac{1}{1-\alpha}\int_\alpha^1 \mathrm{VaR}_\gamma(X)\,d\gamma \tag{19}$$

where the value-at-risk (VaR) is defined as $\mathrm{VaR}_\gamma = F^{-1}(\gamma) = \inf\{y : F(y) \ge \gamma\}$ with $F^{-1}(\gamma)$ inverse of the cumulative distribution function $F(y) = \Pr\{X \le y\}$ [27]. Observing that

$$\alpha\,\mathrm{CVaR}^L_\alpha(X) + (1-\alpha)\,\mathrm{CVaR}^R_\alpha(X) = \mathrm{E} \tag{20}$$

follows

$$\mathrm{CVaR}^L_\alpha(X) = \frac{1}{\alpha}\,\mathrm{E} - \frac{1-\alpha}{\alpha}\,\mathrm{CVaR}^R_\alpha(X) \tag{21}$$

Returning to the analysis of Fig. 14, which was obtained by collecting the populations at the 68-th generation, the advantage of the $N = 8$ in the left tail of the probability distribution focused on the QoI minimum values appears evident, and this advantage is well evidenced by the corresponding CVaR^L values. The right tail of the distribution instead shows a lower dispersion of high QoI values in the case of $N = 5$. This may indicate convergence or a premature stagnation of the $N = 5$ parameterization during the search process for the optimum. Note, then, that although the CVaR^R values are very similar for the $N = 5$ and $N = 8$, the greater difference between VaR and CVaR^R in the case of $N = 8$ indicates that the degree of diversity of the population is still acceptable in this case.

The observation of Fig. 15, reporting CVaR^R in ordinate logarithmic scale, shows that the dispersion of the initial populations is much higher for the $N = 5$ and 8 parameterization than for the original $M = 20$. This is in most cases because the $N = 5$ and 8 design spaces initially generate more "extreme" shapes that do not respect the geometric constraints of the optimization problem or that cause the CFD solver to diverge. This is certainly a shortcoming of the search space compression technique that might require filtering based on either geometric or physical characteristics of the problem [14,31]. Around the twentieth generation, instead, the situation reverses, and the CVaR^R trends show that the $N = 5$ and 8 reduced-design space reach convergence and decrease the diversity before the original $M = 20$ parameterization.

Fig. 16 top shows the CVaR^L as a function of CMA-ES generations for each of the coding used. The lower values of $M = 20$ original design space in the first generations show how the exploiting capabilities of the latter are prevalent in the first phase of optimization, while $N = 5$ and 8 parameterizations seem to favor a greater exploratory capacity of the design space. Fig. 16 bottom, which is a closeup on the ordinate scale, highlights that around generation 60, $N = 5$ and $M = 20$ show signs of population convergence on local minima, while $N = 8$ still seems capable of allowing exploitation and improving the optimum before reaching convergence.

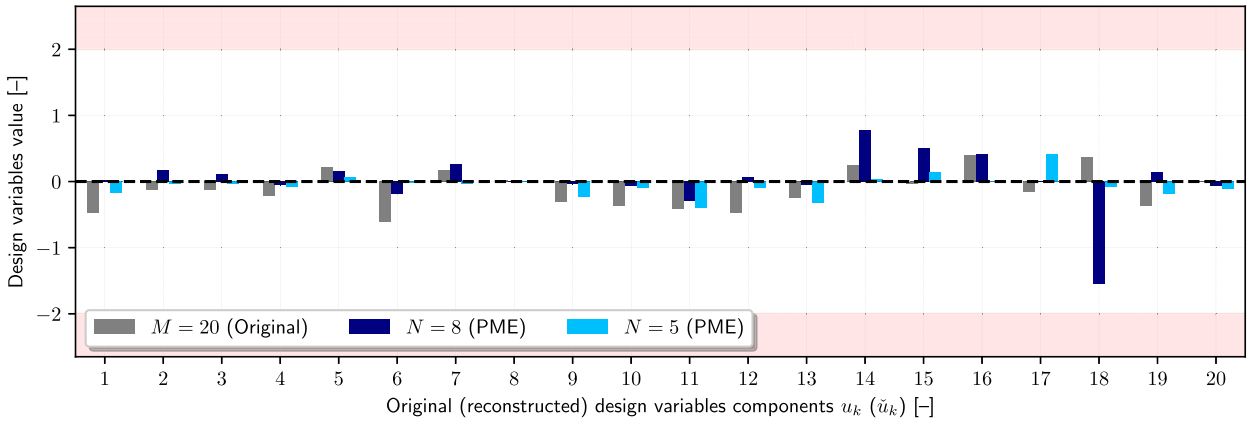

Fig. 11. Comparison of optimal design variable (best) values.

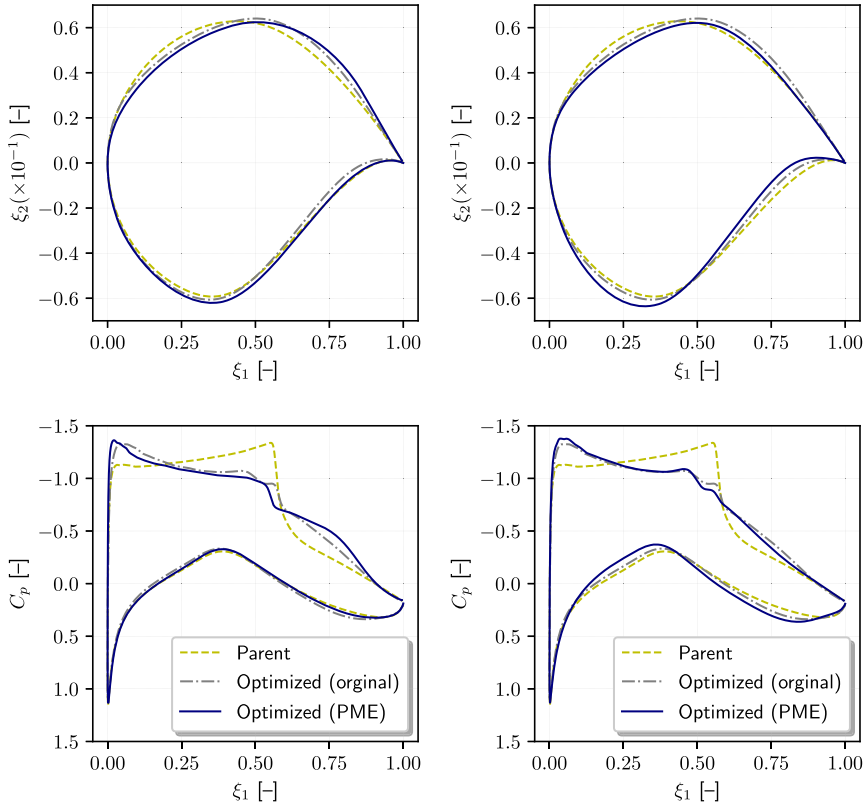

(a) $N = 5$ (b) $N = 8$

Fig. 12. Airfoil shape (top) and associated pressure coefficient (bottom) comparison between parent and optimized airfoils in the original and reduced design space.

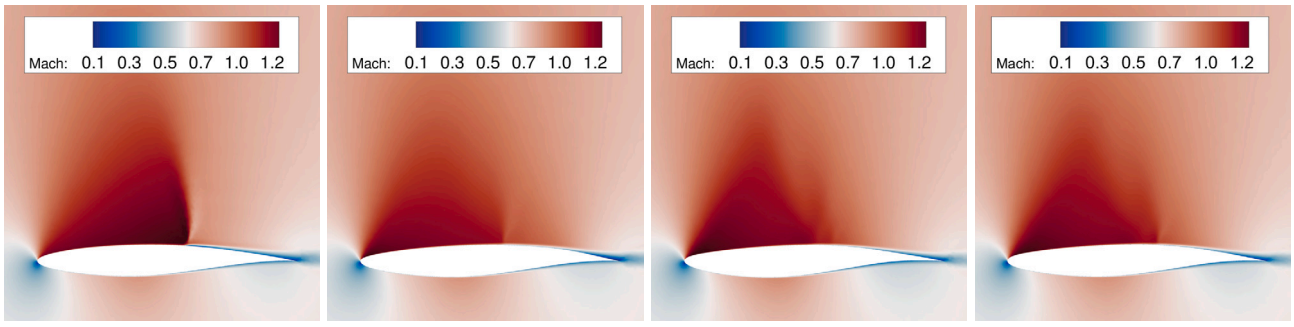

(a) Parent (b) $N = 5$ (PME) (c) $N = 8$ (PME) (d) $M = 20$

Fig. 13. Mach field comparison between parent and optimized airfoils.

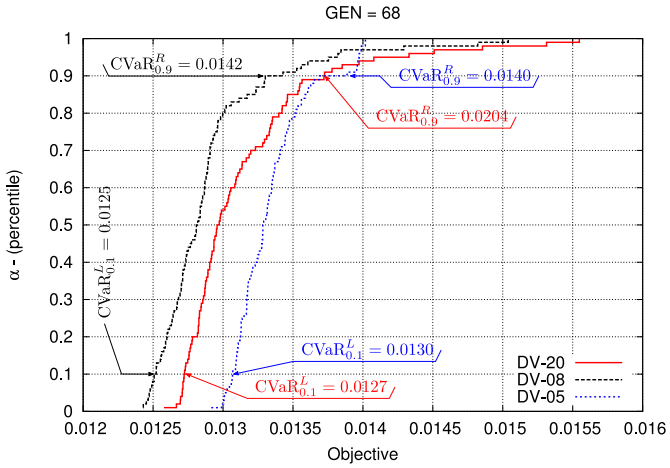

Fig. 14. Empirical distribution functions obtained for the different design variables parameterizations at the 68-th generation.

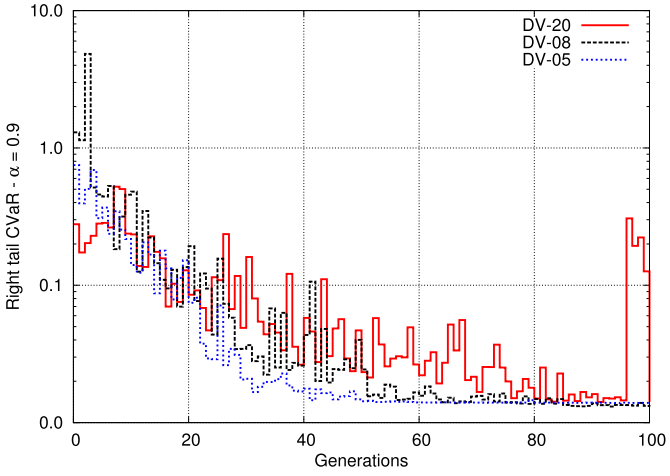

Fig. 15. Right tail CVaR^R in logarithmic scale as a function of CMA-ES generations.

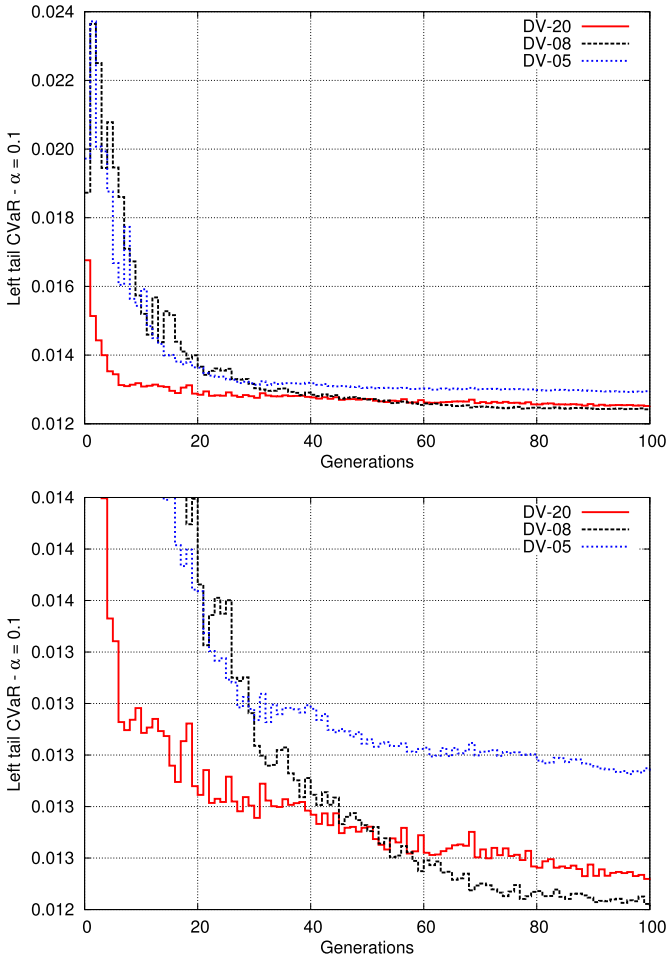

Fig. 16. Left tail (top) CVaR^L as a function of CMA-ES generations and (bottom) closeup.

6. Conclusions

In this study, the shape optimization of the RAE-2822 airfoil under transonic conditions has been explored using the parametric model embedding (PME) technique. By integrating PME into the design optimization process, the design-space dimensionality has been successfully reduced while maintaining a clear connection to the original parameters. This approach mitigated the curse of dimensionality and facilitated a more efficient optimization process.

The results demonstrate that the PME method is effective in preserving the essential characteristics of the original design space, enabling accurate reconstructions and meaningful shape modifications. Specifically, the optimization conducted in the PME-reduced design space with $N = 8$ retained at least 99% of the geometric variance and yielded an optimized airfoil with reduced drag and improved aerodynamic performance compared to both the original and other reduced spaces.

The CMA-ES algorithm was employed to handle the optimization process, and multiple independent runs ensured the statistical robustness of the results. The optimized designs showed significant improvements in terms of shock wave mitigation and smoother pressure distributions along the airfoil surface. Additionally, the statistical analysis helped to understand the advantages and disadvantages of different levels of parameter space compression.

The PME technique can be applied without substantial modifications to handle three-dimensional geometries, such as wings and full aircraft configurations, to evaluate its performance in more complex design spaces. Furthermore, PME direct integrability into CAD software can potentially streamline the design optimization process in industrial applications. However, collaborating with industry partners to apply PME in real-world projects is essential to validate its practical benefits and identify any additional requirements for industrial adoption.

Finally, the application of PME to physics-informed [30,31] and physics-related [14,15] formulations, as well as to nonlinear dimensionality reduction methods [7], is a viable approach to address the limitations of linear approximations of PCA when dealing with strong nonlinearities in shape parameterization or underlying physics. This PME analysis will help determine when it is appropriate to introduce physics-based or shape-based constraints in the compressed parameterization, further enhancing the effectiveness of the optimization process.

CRediT authorship contribution statement

Andrea Serani: Writing – review & editing, Writing – original draft, Visualization, Validation, Software, Methodology, Investigation, Formal analysis, Conceptualization. **Matteo Diez:** Writing – review & editing, Supervision, Methodology, Funding acquisition. **Domenico Quagliarella:** Writing – review & editing, Visualization, Software, Investigation, Formal analysis, Data curation.

Declaration of competing interest

The authors declare that they have no known competing financial interests or personal relationships that could have appeared to influence the work reported in this paper.

Data availability

Data will be made available on request.

Acknowledgements

The work was conducted in collaboration with the NATO task group AVT-331 on “Goal-driven, multi-fidelity approaches for military vehicle system-level design”. CNR-INM authors are grateful to the US Office of Naval Research Global for its support through grants N62909-18-1-2033 and N62909-21-1-2042. The work carried out by CIRA was supported by the internal project OPTIWING (OPTImization for WINg Generation).

References

[1] C. Acerbi, D. Tasche, Expected shortfall: a natural coherent alternative to value at risk, Econ. Notes 31 (2002) 379–388, https://doi.org/10.1111/1468-0300.00091.
[2] C.B. Allen, D.J. Poole, T.C. Rendall, Wing aerodynamic optimization using efficient mathematically-extracted modal design variables, Optimization and Engineering 19 (2018) 453–477, https://doi.org/10.1007/s11081-018-9376-7.
[3] R.E. Bellman, et al., Dynamic Programming, Cambridge Studies in Speech Science and Communication, Princeton University Press, Princeton, 1957.
[4] Y. Bengio, A. Courville, P. Vincent, Representation learning: a review and new perspectives, IEEE Trans. Pattern Anal. Mach. Intell. 35 (2013) 1798–1828, https://doi.org/10.1109/TPAMI.2013.50.
[5] P.S. Beran, D. Bryson, A.S. Thelen, M. Diez, A. Serani, Comparison of multi-fidelity approaches for military vehicle design, in: AIAA AVIATION 2020 FORUM, 2020, p. 3158.
[6] D. Cinquegrana, E. Iuliano, Investigation of adaptive design variables bounds in dimensionality reduction for aerodynamic shape optimization, Comput. Fluids 174 (2018) 89–109, https://doi.org/10.1016/j.compfluid.2018.07.012.
[7] D. D’Agostino, A. Serani, E.F. Campana, M. Diez, Nonlinear methods for design-space dimensionality reduction in shape optimization, in: 3rd International Conference on Machine Learning, Optimization, and Big Data, MOD 2017, Volterra, Italy, 2017.
[8] M. Diez, E.F. Campana, F. Stern, Design-space dimensionality reduction in shape optimization by Karhunen–Loève expansion, Comput. Methods Appl. Mech. Eng. 283 (2015) 1525–1544, https://doi.org/10.1016/j.cma.2014.10.042.
[9] D. Gaudrie, R. Le Riche, V. Picheny, B. Enaux, V. Herbert, Modeling and optimization with Gaussian processes in reduced eigenbases, Struct. Multidiscip. Optim. 61 (2020) 2343–2361, https://doi.org/10.1007/s00158-019-02458-6.
[10] C. Geuzaine, J.F. Remacle, Gmsh: A 3-D finite element mesh generator with built-in pre- and post-processing facilities, Int. J. Numer. Methods Eng. 79 (2009) 1209–1331, https://doi.org/10.1002/nme.2579.
[11] N. Hansen, The CMA evolution strategy: a comparing review, in: Towards a new evolutionary computation: Advances in the estimation of distribution algorithms, 2006, pp. 75–102.
[12] R. Hicks, P.A. Henne, Wing design by numerical optimization, J. Aircr. 15 (1978) 407–412, https://doi.org/10.2514/3.58379.
[13] K. Hu, Y. Ju, Y. Feng, C. Zhang, A dimension reduction-based multidisciplinary design optimization method for high pressure turbine blades, J. Eng. Gas Turbines Power 144 (2022) 091011, https://doi.org/10.1115/1.4055186.
[14] S. Khan, P. Kaklis, A. Serani, M. Diez, Geometric moment-dependent global sensitivity analysis without simulation data: application to ship hull form optimisation, Comput. Aided Des. 103339 (2022), https://doi.org/10.1016/j.cad.2022.103339.
[15] S. Khan, P. Kaklis, A. Serani, M. Diez, K. Kostas, Shape-supervised dimension reduction: extracting geometry and physics associated features with geometric moments, Comput. Aided Des. 103327 (2022), https://doi.org/10.1016/j.cad.2022.103327.
[16] A.B. Lambe, J.R. Martins, Extensions to the design structure matrix for the description of multidisciplinary design, analysis, and optimization processes, Struct. Multidiscip. Optim. 46 (2012) 273–284, https://doi.org/10.1007/s00158-012-0763-y.
[17] J. Li, M.A. Bouhlel, J.R. Martins, Data-based approach for fast airfoil analysis and optimization, AIAA J. 57 (2019) 581–596, https://doi.org/10.2514/1.J057129.
[18] J. Li, X. Du, J.R. Martins, Machine learning in aerodynamic shape optimization, Prog. Aerosp. Sci. 134 (2022) 100849, https://doi.org/10.1016/j.paerosci.2022.100849.
[19] J. Li, M. Zhang, Adjoint-free aerodynamic shape optimization of the common research model wing, AIAA J. 59 (2021) 1990–2000, https://doi.org/10.2514/1.J059921.
[20] J.L. Li, Y. Zhang, B.b. Zhu, B. Pang, G. Chen, The aerodynamic optimization of hypersonic vehicles with the proper-orthogonal-decomposition-based CST method, Aerosp. Sci. Technol. (2024) 109295, https://doi.org/10.1016/j.ast.2024.109295.
[21] D.A. Masters, N.J. Taylor, T. Rendall, C.B. Allen, D.J. Poole, Geometric comparison of aerofoil shape parameterization methods, AIAA J. 55 (2017) 1575–1589, https://doi.org/10.2514/1.J054943.
[22] D.C. Montgomery, G. Weatherby, Factor screening methods in computer simulation experiments, Technical Report, Institute of Electrical and Electronics Engineers (IEEE), 1979.
[23] F. Palacios, J. Alonso, K. Duraisamy, M. Colonno, J. Hicken, A. Aranake, A. Campos, S. Copeland, T. Economon, A. Lonkar, T. Lukaczyk, T. Taylor, Stanford University Unstructured (SU^2): an open-source integrated computational environment for multi-physics simulation and design, in: 51st AIAA Aerospace Sciences Meeting Including the New Horizons Forum and Aerospace Exposition, American Institute of Aeronautics and Astronautics, 2013.
[24] D.J. Poole, C.B. Allen, T.C. Rendall, High-fidelity aerodynamic shape optimization using efficient orthogonal modal design variables with a constrained global optimizer, Comput. Fluids 143 (2017) 1–15, https://doi.org/10.1016/j.compfluid.2016.11.002.
[25] D.J. Poole, C.B. Allen, T.C. Rendall, Metric-based mathematical derivation of efficient airfoil design variables, AIAA J. 53 (2015) 1349–1361, https://doi.org/10.2514/1.J053427.
[26] D.J. Poole, C.B. Allen, T.C. Rendall, Efficient aeroelastic wing optimization through a compact aerofoil decomposition approach, Struct. Multidiscip. Optim. 65 (2022) 81, https://doi.org/10.1007/s00158-022-03174-4.
[27] D. Quagliarella, Value-at-Risk and Conditional Value-at-Risk in Optimization Under Uncertainty, Springer International Publishing, Cham, 2019, pp. 541–565.
[28] D. Quagliarella, D. Clark, D. Bryson, P. Beran, A. Thelen, L. Mainini, S. Yildiz, M. Nikbay, E. Minisci, P. Leyland, A. Serani, M. Diez, Reproducible industrial multifidelity optimization benchmark problems for air, space, and sea vehicles, in: Research Workshop AVT-354 on Multifidelity Methods for Military Vehicle Design, 2022.
[29] R.T. Rockafellar, S. Uryasev, Optimization of conditional value-at risk, J. Risk 2 (2000) 21–41, https://doi.org/10.21314/JOR.2000.038.
[30] A. Serani, E.F. Campana, M. Diez, F. Stern, Towards augmented design-space exploration via combined geometry and physics based Karhunen-Loève expansion, in: 18th AIAA/ISSMO Multidisciplinary Analysis and Optimization Conference (MA&O), AVIATION 2017, Denver, USA, June, 2017, pp. 5–9.
[31] A. Serani, D. D’Agostino, E.F. Campana, M. Diez, Assessing the interplay of shape and physical parameters by unsupervised nonlinear dimensionality reduction methods, J. Ship Res. 64 (2020) 313–327, https://doi.org/10.5957/JOSR.09180056.
[32] A. Serani, M. Diez, Parametric model embedding, Comput. Methods Appl. Mech. Eng. 404 (2023) 115776, https://doi.org/10.5957/JOSR.09180056.
[33] A. Serani, M. Diez, A survey on design-space dimensionality reduction methods for shape optimization, arXiv preprint, arXiv:2405.13944, 2024.
[34] A. Serani, M. Diez, D. Quagliarella, Efficient shape optimization via parametric model embedding, in: AIAA SCITECH 2023 Forum, 2023, p. 1273.
[35] A. Serani, F. Stern, E.F. Campana, M. Diez, Hull-form stochastic optimization via computational-cost reduction methods, Eng. Comput. 38 (2022) 2245–2269, https://doi.org/10.1007/s00366-021-01375-x.
[36] I.M. Sobol, Global sensitivity indices for nonlinear mathematical models and their Monte Carlo estimates, Math. Comput. Simul. 55 (2001) 271–280, https://doi.org/10.1016/S0378-4754(00)00270-6.
[37] P. Spalart, S. Allmaras, A one-equation turbulence model for aerodynamic flows, in: 30th Aerospace Sciences Meeting and Exhibit, 1992, p. 439.
[38] D.J. Toal, N.W. Bressloff, A.J. Keane, C.M. Holden, Geometric filtration using proper orthogonal decomposition for aerodynamic design optimization, AIAA J. 48 (2010) 916–928, https://doi.org/10.2514/1.41420.
[39] X. Wu, L. Ma, Z. Zuo, High-dimensional aerodynamic shape optimization framework using geometric domain decomposition and data-driven support strategy for wing design, Aerosp. Sci. Technol. 149 (2024) 109152, https://doi.org/10.1016/j.ast.2024.109152.
[40] X. Wu, W. Zhang, X. Peng, Z. Wang, Benchmark aerodynamic shape optimization with the POD-based CST airfoil parametric method, Aerosp. Sci. Technol. 84 (2019) 632–640, https://doi.org/10.1016/j.ast.2018.08.005.
[41] T. Xing, F. Stern, Factors of safety for Richardson extrapolation, J. Fluids Eng. 132 (2010) 061403, https://doi.org/10.1115/1.4001771.
[42] W. Yamazaki, Efficient multi-objective shape optimization using proper orthogonal decomposition with variable fidelity concept, J. Adv. Mech. Des. Syst. Manuf. 14 (2020), https://doi.org/10.1299/jamdsm.2020jamdsm0019.
[43] H. Yang, Q. Yang, Z. Mu, X. Du, L. Chen, Optimal design of three-dimensional circular-to-rectangular transition nozzle based on data dimensionality reduction, Energies 15 (2022) 9316, https://doi.org/10.3390/en15249316.
[44] D. Yanhui, W. Wenhua, P. Zhang, T. Fulin, F. Zhaolin, Z. Guiyu, L. Jiaqi, Performance improvement of optimization solutions by POD-based data mining, Chin. J. Aeronaut. 32 (2019) 826–838, https://doi.org/10.1016/j.cja.2019.01.014.
[45] Q. Yasong, B. Junqiang, L. Nan, W. Chen, Global aerodynamic design optimization based on data dimensionality reduction, Chin. J. Aeronaut. 31 (2018) 643–659, https://doi.org/10.1016/j.cja.2018.02.005.
[46] K. Yonekura, O. Watanabe, A shape parameterization method using principal component analysis in applications to parametric shape optimization, J. Mech. Des. 136 (2014) 121401, https://doi.org/10.1115/1.4028273.
[47] L. Zhang, D. Mi, C. Yan, F. Tang, Multidisciplinary design optimization for a centrifugal compressor based on proper orthogonal decomposition and an adaptive sampling method, Appl. Sci. 8 (2018) 2608, https://doi.org/10.3390/app8122608.